Determination of the optical properties of a two-layer tissue model by detecting photons migrating at progressively increasing depths

Yasser S. Fawzi, Abo-Bakr M. Youssef, Mohamed H. El-Batanony, and Yasser M. Kadah

We have investigated a method for solving the inverse problem of determining the optical properties of a two-layer turbid model. The method is based on deducing the optical properties (OPs) of the top layer from the absolute spatially resolved reflectance that results from photon migration within only the top layer by use of a multivariate calibration model. Then the OPs of the bottom layer are deduced from relative frequency-domain (FD) reflectance measurements by use of the two-layer FD diffusion model. The method was validated with Monte Carlo FD reflectance profiles and experimental measurements of two-layer phantoms. The results showed that the method is useful for two-layer models with interface depths of >5 mm; the OPs were estimated, within a relatively short time (<1 min), with a mean error of <10% for the Monte Carlo reflectance profiles and with errors of <25% for the phantom measurements.

OCIS codes: 170.5280, 170.7050, 170.3660, 170.4580.

1. Introduction

The optical properties, namely, absorption and scattering coefficients, of tissue provide useful and critical information about tissue chromospheres, physiological functions, and structure. Thus the measurement of these optical properties can be useful in various medical and clinical applications, for example, quantification of photosensitized uptakes in photodynamic therapy, monitoring of blood glucose, and measurement of cerebral and muscle oxygenation. Great effort has recently been devoted to the determination of the optical properties of biological tissue by noninvasive diffuse reflectance measurements, as first proposed by Groenhuis *et al*.[1] In this method a beam of monochromatic laser light is incident upon the tissue's surface, and the optical properties of the tissue are deduced from the measured reflectance profile by use of inverse calculations in a suitable transport model (inverse problem). Various measurement arrangements and inverse-problem algorithms, including spatially resolved cw measurements,[2–5] frequency-domain measurements,[6–8] and time-resolved measurements,[9,10] have by developed by a number of researchers. The criteria for validity of such measurement arrangements and inverse-problem algorithms in actual clinical applications are determined mainly by the accuracy of the estimated optical properties, the time needed to extract and estimate such optical properties, and the ability to account for nonhomogeneous and layered tissue structure. Although most tissues have layered structures, for many instrumentation and measurement techniques it has been assumed that the tissue is homogenous.

Tissue architecture and its effect on estimated optical properties have been studied both theoretically[11,12] and experimentally.[13–15] Other studies investigated the effect of overlying layers on the perceived volume and on the detected signal of deep tissues (the brain).[16,17] The effect of overlaying layers on muscle oxygenation measurements was also studied.[18] Few systems and inverse-problem methods have been used to investigate the reflectance measured from multilayer tissues, in particular, with a two-layer model.[14,19,20] Kienle *et al*.[13,14] developed

The authors are with Cairo University, Cairo, Egypt. Y. S. Fawzi (laser@internetegypt.com) is with the Department of Laser Applications in Medicine, National Institute of Enhanced Laser Sciences; A.-B. M. Youssef and Y. M. Kadah are with the Department of Biomedical Engineering, Faculty of Engineering; and M. H. El-Batanony is with the Department of Surgery, Faculty of Medicine.

Received 4 October 2002; revised manuscript received 31 March 2003.

0003-6935/03/316398-14$15.00/0

an absolute spatially resolved reflectance-measuring system, using a CCD detector to study multilayer turbid media, and described a two-layer frequency-domain (FD) diffusion model for data analysis.[14] Pham *et al*.[19] developed a system of FD planar photon density waves that uses modulation frequencies ranging from 10 to 1500 MHz. Although the time needed for deducing the optical properties was short, at least two parameters had to be known *a priori* for reasonable results to be achieved. Alexandrakis *et al*.[20–22] concentrated on the problem of deducing the five optical properties, including interface depth, of a two-layer model that simulates a skin layer (1.5–4 mm) and the semi-infinite underlying fat or muscle layer. They proposed a hybrid Monte Carlo diffusion model[21] and developed a spatially resolved FD reflectance-measurement system for deducing these five optical properties.[22] However, their experimental results still showed significant differences from the theoretical predictions of the hybrid model.

In this paper we investigate the approach of deducing the optical properties of two-layer tissues by detecting and analyzing the reflectance that results from photons propagated at progressively increasing depths such that each layer is characterized sequentially. Although the approach can be extended to multilayer models in our study we have investigated only a two-layer model that has a finite top-layer thickness (2–10 mm) and a semi-infinite bottom layer. Such a two-layer model has been used successfully to model many layered-tissue structures such as skin (2–4 mm) and underlying fat,[19,20] brain and overlying skull (~10 mm),[16] and muscle and overlying fat and skin (4–10 mm).[18] We developed diffuse reflectance-measurement apparatus that measures spatially resolved cw and FD diffuse reflectance by using phantoms to simulate the optical properties of the two-layer tissue. In Section 2 we describe the proposed method and the procedure used for solving the inverse problem of deducing the properties of the two-layer tissue model. In Section 3 we give a detailed description of the apparatus and the measuring probe design and of the measurement and the calibration procedures. In Section 4 we clarify and discuss the intrinsic limits of the technique for deducing the optical properties of the two-layer medium. This was done through validation of the method using low noise Monte Carlo simulated FD reflectance profiles (ideal measurements). Finally we present and discuss the results of experimental measurements performed on a number of two-layer solid phantoms. The uses and limitations of the method are discussed in detail.

2. Theory

A. Method

Our measuring method is based on a simple concept: that the addressable depths of photons in a medium increase with increasing source–detector spacing.[23,24] Thus the probed depth inside tissue can be controlled by manipulation of the detector position. A quantitative estimation of the relation between the detector's position relative to the incident source and its sensitivity to the optical properties at specific depths inside the tissue is obtained by use of a spatial-sensitivity profile.[16,25] This sensitivity profile indicates the change in attenuation at a certain spatial point (x, y, z) inside the tissue to the total detected signal. To determine the contribution of the attenuation change at a certain depth z inside the tissue we define the depth-sensitivity profile as follows:

$$E_i(z; d_0, d_1) = I_i(d_0, d_1)n, \tag{1}$$

where d_1 is the location of the detection fiber, d_0 is the location of the source fiber, n is the number of passages of the photon through depth z, and I_i is the output intensity of the ith photon. The depth-sensitivity profile for m scattered photons is then obtained from

$$E(z; d_0, d_1) = \sum_{i=0}^{m} E(z; d_0, d_1). \tag{2}$$

Using this representation and using Monte Carlo simulation, we generated depth-sensitivity profiles for several detector positions along radial distances 0.5–30 mm. Figure 1 shows an example of this kind of profile for a number of detector positions. From these depth-sensitivity profiles we define the maximum depth probed by a detector at position d as the depth inside the tissue that has a sensitivity of $<5\%$ of the total signal measured by the detector. A curve that shows the maximum probe depth for several radial detector positions is shown in Fig. 2. Thus from knowledge of the thickness of the tissue layer investigated we can determine the limiting detector position for probing certain layer thicknesses inside

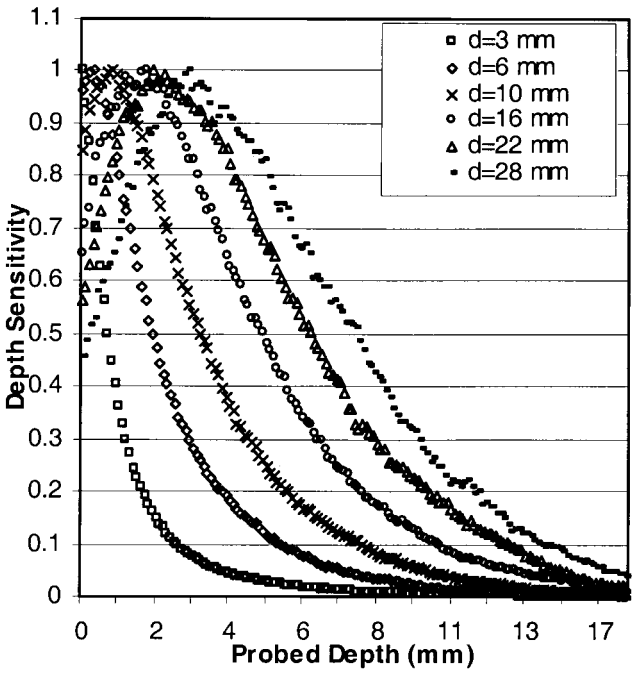

Fig. 1. Depth-sensitivity profiles for several source–detector distances.

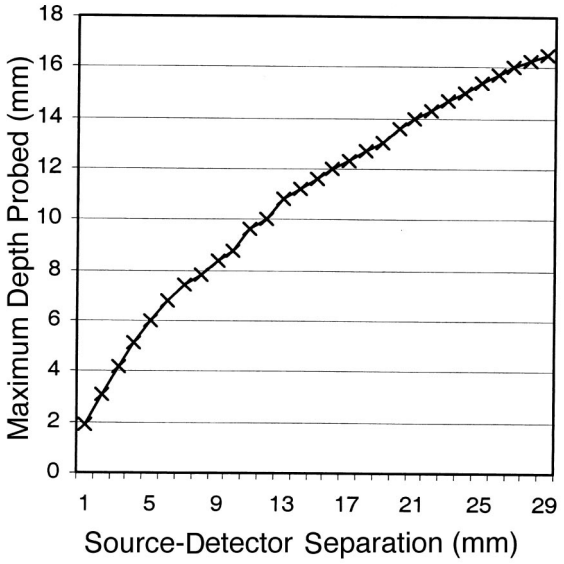

Fig. 2. Maximum depth probed versus source–detector distances.

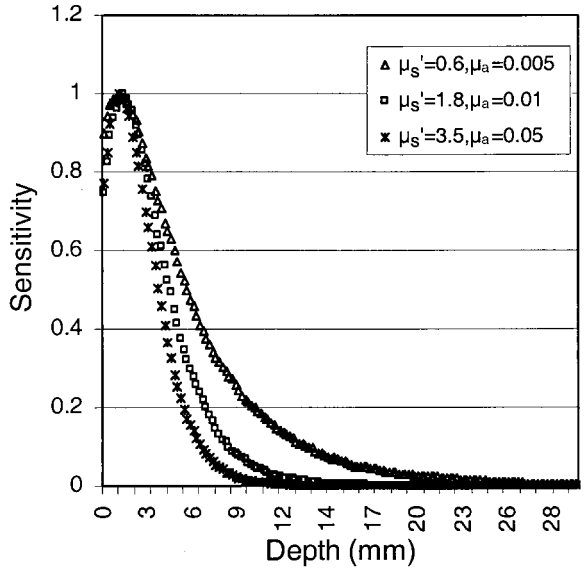

Fig. 3. Depth-sensitivity profiles for several optical properties [mm^{-1}] investigated with the same source–detector distance, d = 13 mm.

the tissue. In practice, the layer thickness is usually known *a priori* from the general anatomy of the tissue or from ultrasound measurements with errors of <20%. Thus, based on knowledge of the thickness of the top layer of a two-layer turbid medium, we could determine (with >95% confidence) from Figs. 1 and 2 the limiting detector position $D1$ such that the detected reflectance for any detector position at $d < D1$ will result from photons propagated mainly within the top layer only. The problem then becomes deducing the top layer's optical properties from fitting of the reflectance data confined to $D1$ by use of a one-layer model and deducing the bottom layer's optical properties from fitting of the reflectance data at detector(s) $d > D1$ by using an appropriate two-layer model. The reflectance data used in the fitting were spatially resolved cw reflectance measurements and spatially resolved FD reflectance for obtaining the top-layer and bottom-layer optics, respectively. In particular, we used absolute spatially resolved cw reflectance along radial distances in the range 0.5 mm, D = 1 mm to estimate the top layer's optical properties. For FD reflectance, which is needed for the bottom-layer optics, we used the relative phase-delay data and the relative cw reflectance at a number of detectors located in the diffusion propagation regime (i.e., at $d > 5$ mm from the source) such that the use of the analytical diffusion approximation model is valid. The use of such combined absolute cw and relative FD reflectance measurements to deduce top- and bottom-layer optical properties, respectively, was motivated by the results of previous research,[7,14] which showed that use of spatially resolved reflectance measurements is best for superficial (top) layers (1.5–5 mm). The use of FD measurements, however, was found to be more efficient for estimating the properties of the deep (bottom) semi-infinite layer.[14,22] It should be noted, however, that the maximum depth probed for a given source–detector distance $D1$ depended on the optical properties of the tissue.[24] As shown in Fig. 3 for the same detector position, the maximum depth probed is increased for tissue with low absorption and scattering properties. Thus, to use the proposed method to investigate tissues with optical properties within a certain range, for example, $0.005 < \mu_a < 2.0\ mm^{-1}$ and $0.6 < \mu_b < 3.5\ mm^{-1}$, which are typical biological ranges, one should base the limiting source–detector distance $D1$ on the lowest optical properties in the designated range.

Although it was not investigated in this study, the approach described above could be extended to a multilayer tissue model. For example, to investigate an n-layer tissue model we could determine from Fig. 2 the limiting detector positions ($d1$, $d2$, $d3$, . . . , dn) for layers (1, 2, 3, . . . n), respectively. The method then proceeded to fit the optical properties of the first layer to the measured reflectance data in the FD or in the steady-state domain confined to detector position $d1$ by a one-layer (homogeneous) model. The optical properties of the second layer were then obtained by fitting of the reflectance data confined to detector position $d2$ by use of a two-layer model with the first layer's optical properties known *a priori*. We obtained the optical properties of the third layer, from reflectance data confined to $d3$, by assuming a three-layer model with the first and second layers' optical properties known *a priori*. The same applies for any layer n in an n-layer model with only the optical properties of layer n unknown during the fitting procedure. A suggested arrangement for extracting the optical properties of multilayer (>3 layers) tissues is to use this method with one limiting detector position for each layer and to generate frequency-resolved reflectance measurements (100–1000 MHz) such that

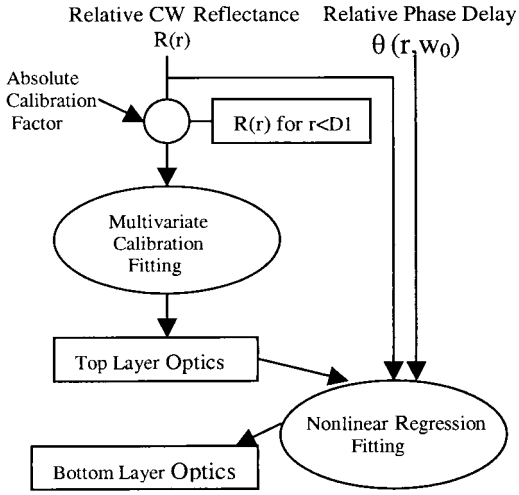

Fig. 4. Inverse-problem algorithm.

each layer's optical properties can be deduced from the reflectance measured at this detector only.

B. Inverse-Problem Analysis

For extraction of the top-layer optics from cw reflectance measurements we used the ordinary least-squares multivariate calibration method.[26] The bottom-layer optics was then extracted by fitting of the two-layer FD diffusion equation to the FD reflectance measurements, with the top layer's optical properties known *a priori*. The inverse-problem algorithm flow chart is shown in Fig. 4. Monte Carlo simulations[27] were performed to generate the data base of reflectance profiles that constitutes the calibration model. The Monte Carlo data base of reflectance profiles was generated by multilayer Monte Carlo simulation, which has been described in detail elsewhere[28] and also was used for generating the depth-sensitivity profiles and for generating noisy FD reflectance profiles (see Subsection 4.A below). For FD reflectance, the Monte Carlo simulation was solved in the time domain and inversely transformed to the FD by a fast-Fourier-transform algorithm. The spatial resolution was 0.2 mm, and the temporal resolution was 2.5 ps. The tissue's index of refraction was assumed to have a fixed value of $n = 1.4$. The refractive-index mismatch boundary condition was accounted for by use of Fresnel Low when the calibration model data base was generated. We used the refractive index of air ($n = 1$) and that of the probe surface ($n = 1.5$) in fitting the low-noise Monte Carlo reflectance profiles and the experimental measurements, respectively. The simulation also accounts, through convolution and integration, for the known finite size of the source and the detector fibers used in the experiment. The data base of reflectance profiles was generated for the source–detector arrangements and geometries identical to that of the measuring probe (see Subsection 3.B below).

The calibration model data base consisted of a matrix of 15×15 combinations (300 pairs) of absorption and scattering coefficients, which we used to equally scan the optical properties of the ranges used in this study ($0.005\ \text{mm}^{-1} < \mu_a < 2\ \text{mm}^{-1}$ and $0.6\ \text{mm}^{-1} < \mu_{s'} < 3.5\ \text{mm}^{-1}$). Powell's quadratically convergent method[29] was used for fast and efficient searching of the calibration model's reflectance data base for the values of absorption and scattering coefficients that give the least-squares fit (best match). The values between the simulated μ_a and $\mu_{s'}$ pairs were obtained by cubic spline interpolation.[29] The least-squares fitting search was confined to reflectance values at $r < D1$. The bottom layer's optical properties were obtained from fitting of the two-layer FD diffusion equations, with the top-layer optics known *a priori*, to the FD reflectance measurements. The Marquardt nonlinear least-squares fitting method[29] was used for fitting the two-layer FD model. This method uses the inverse-Hessian method far from the minimum, switching continuously to the steepest-descent method as the minimum is approached. The method works well in practice and has been used in the field of tissue optics as well.[11,12,14]

The two-layer FD diffusion model used in the fitting procedures (the forward model) was used earlier by many authors to model photon propagation in the diffuse regime.[14,20,22] A brief description of the model is presented to assist the reader: The diffusion equations for the fluence rate of a two-layer medium from an intensity-modulated source are given by

$$D_1\nabla^2\Phi_1(r,\omega) - \left(\mu_{a1} + j\frac{w}{c_0}\right)\Phi_1(r,\omega) = -\delta(x, yz - z_0)\exp\left(j\frac{w}{c_m}r\right) \qquad 0 \le z \le l, \quad (3)$$

$$D_2\nabla^2\Phi_2(r,\omega) - \left(\mu_{a2} + j\frac{w}{c_0}\right)\Phi_2(r,\omega) = 0 \qquad l \le z, \quad (4)$$

where $r = (x^2 + y^2 + z^2)^{1/2}$; Φ_i is the fluence rate for layers $i = 1, 2$; $D_i = \frac{1}{3}(\mu_{ai} + \mu_{si}')^{-1}$ is the diffusion constant; $\omega = 2\pi f$ is the modulation frequency; and c_m is the speed of light. The refractive index is assumed to be the same for both layers and to be equal to 1.4. According to Kinel *et al.*,[14] Eqs. (3) and (4) are transformed into ordinary differential equations by use of a two-dimensional Fourier transform and solved to yield the fluence solution in frequency space coordinates $\phi_1(s, z, \omega)$ and $\phi_2(s, z, \omega)$ for layers 1 and 2, respectively, by use of the following boundary conditions[20]: zero fluence rate at the extrapolated boundary, finite photon fluence rate as $r \to \infty$, and continuity of fluence rate and flux at the boundary between the two layers.

The real-space (Fourier inversion) fluence solution (at $z = 0$) is thus obtained from[14]

$$\Phi_1(r, z = 0) = \frac{1}{2\pi}\int_0^\infty \varphi_1(z = 0)sI_0(sr)\mathrm{d}s, \quad (5)$$

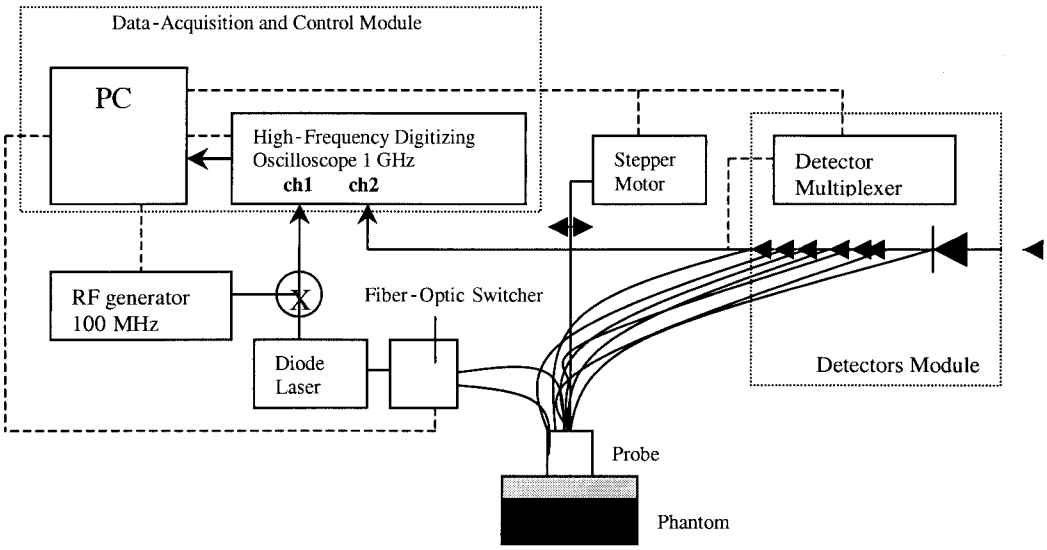

Fig. 5. Schematic of the apparatus.

where I_0 is the zeroth-order Bessel function. Spatially resolved reflectance $R(r)$ is obtained from the integral of the radiance over the backward hemisphere. For fitting the low-noise Monte Carlo reflectance profiles we assumed a tissue–air reflective-index mismatch, and we thus obtained the spatially resolved reflectance from[14]

$$R(r, \omega) = 0.118\Phi_1(r, z = 0) + 0.306D \times {}_1 \frac{\partial}{\partial z} \Phi_1(r, z, \omega)\bigg|_{z=0}. \quad (6)$$

For fitting the experimental measurements we assumed a matched boundary condition, and the spatially resolved reflectance was obtained from[20]

$$R(r, \omega) = \tfrac{1}{4}\, \Phi_1(r, z = 0) + \tfrac{1}{2}\, D_1 \frac{\partial}{\partial z} \Phi_1(r, z, \omega)\bigg|_{z=0}. \quad (7)$$

The phase of the detected light relative to the source is thus obtained from

$$\theta(r, \omega) = \tan^{-1} \frac{\mathrm{Im}[R(r, \omega)]}{\mathrm{Re}[R(r, \omega)]}. \quad (8)$$

3. Experiment

A. Measuring Apparatus

The measuring apparatus was designed to combine both spatially resolved continuous reflectance and spatially resolved phase-delay measurements. A schematic view of the apparatus is shown in Fig. 5. The apparatus is basically a homodyne digital phase-modulation system[31] operating at 100 MHz and modified to measure the cw reflectance from the top layer separately.

The apparatus includes a laser module in which a diode laser (660 nm, 20 mW; from SLI, Inc.) was used as the incident light source. The light from the diode laser was focused, through an electronic fiber optic switcher, into two multimode optical fibers with core diameters of ~250 μm and a N.A. of 22. The diode laser was electronically driven to work in continuous mode (dc) or in a modulated mode (ac). The modulation frequency was controlled by a 100-MHz oscillator.

A detector module is included in the apparatus: Six photodiodes and one high-gain photodiode (International Light, Ltd.) were used for measuring the reflected light signal. Each of the six photodiode detectors was connected to a low-loss transmission fiber (New Port, Inc.; core, ~400 μm; N.A., 0.25) for collecting the top-layer reflectance from the surfaces of the phantoms or tissues. The high-gain photodiode, which matches the sensitivity of a photomultiplier tube using the stability of silicon, was used to measure the spatially resolved FD reflectance data (relative phase and cw reflectance) through a fiber bundle (Edmund, Inc.; 2-mm diameter). The six detectors were connected, by an electronic multiplexer to switch among the detectors, to a current radiometer with a wide dynamic range. The detector fibers were mounted in a measuring probe, which was controlled by a stepper motor (as described in Subsection 3.B below).

The high-frequency digitizing oscilloscope (Tektronix 540) in the apparatus had a built-in analog-to-digital converter to support high-frequency (as high as 1 GHz) sampling to digitize the 100-MHz reference signal received from the oscillator (at ch1; Fig. 5) and the 100-MHz reflectance signal received from the high-gain photodiode detector (at ch2).

A 1000-MHz PC was used for data acquisition and for control of the fiber switcher, the diode laser driver, the stepper motor, the detector multiplexer, and the oscilloscope. The digitized signals were retrieved from the oscilloscope to the PC through a general-

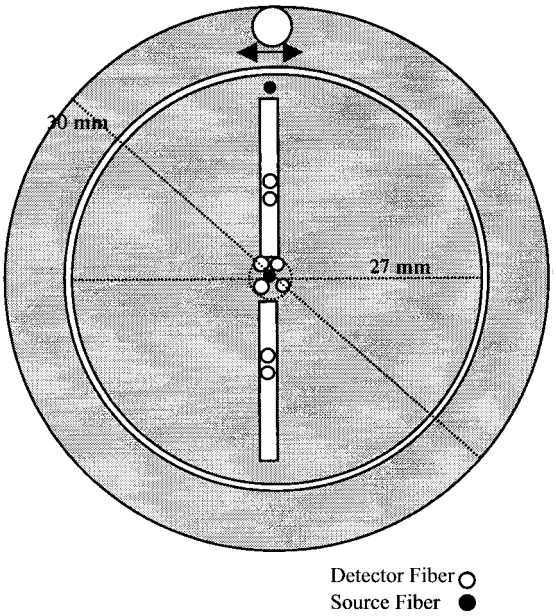

Fig. 6. Probe head: front view.

purpose interface bus. A group-delay estimation algorithm based on the FD was used for phase-delay calculations.[32] This technique estimates the phase shift in terms of the delay encountered whereby this delay is computed by means of linear regression of the phase difference versus the frequency between the two signals in the FD.

B. Probe Design and Reflectance Measurements

The probe is designed to measure both the spatially resolved cw reflectance from the top layer and the FD reflectance from the two layers. As shown in Fig. 6, the probe head has a rotating disk that contains the source and the detector fiber arrangements needed for measurement of the top layer's spatially resolved cw reflectance. The central source fiber was used for the top-layer cw reflectance measurements, but the source fiber near the end of the rotating disk was used for FD reflectance measurements. The spatially resolved FD reflectance (relative phase and relative cw reflectance) could be collected at several distances from 5 to 29 mm, obtained from rotation of the inner disk relative to the high-gain detector fiber bundle. For each inner-disk rotation distance needed for FD reflectance measurements, the top-layer cw reflectance measurements could be repeated. This would allow the same lateral area probed by the FD reflectance measurements to be scanned and local inhomogeneities to be avoided when one is investigating real tissues. Previous research[5,32–34] has shown that, for optimal determination of absorption and scattering properties, spatially resolved reflectance measurements at both near distances (<1 mm) and far distances (>4 mm) are required. However, another design parameter in our case is the probe depth of the detector position, which places an additional constraint on the position of the far detector(s). In this case the position of the far detector is determined from the depth-sensitivity profile and is related to the interface depth of the tissue being investigated. The fiber detector arrangement used for the spatially resolved reflectance measurements of the top layer comprised detectors located at six sites. The first four fiber detectors were arranged at near-source distances of 0.4, 0.7, 1.0, and 1.24 mm such that the probe depth of any of them was less than 2 mm. The fifth and the sixth detector fibers, which are the far detectors, are movable, and their position was determined from the depth-sensitivity profile, relative to the top layer's thickness. The arrangement of two movable fibers was repeated on the other side of the source fiber for geometrical symmetry and to increase the signal-to-noise ratio. At least 20 measurements were repeated to reduce the effects of noise. We eliminated the background effect by setting the detectors to zero before each measurement. The maximum sampling frequency needed for obtaining the data from one measurement was $\sim$1 Hz ($\sim$1-s measurement time). We then used the inverse algorithm to measure the top-layer cw reflectance, the relative phase, and the relative cw reflectance to extract the optical properties as described above.

C. Optical Phantoms

Solid-silicon-based tissue-simulating optical phantoms were used for the calibration as well as for the experimental measurements. The phantoms were composed of silicon host material with embedded Al_2O_3 scattering particles, with added dyes to simulate the absorption characteristics of the tissues. The phantoms were cylindrical in shape, each with radius of 6.5 cm and a height of 6.5 cm. Detailed descriptions of this kind of phantom and its method of manufacture can be found in Ref. 35. The optical phantoms were purchased from Med Light, Inc. Switzerland. One-layer and two-layer phantom sets were purchased; the first set was used mainly for calibration, and the second set was used for the experimental measurements.

D. Calibration

Before fitting the reflectance data obtained experimentally we needed to calibrate the apparatus as follows:

(1) Absolute intensity calibration was needed for measurement of the spatially resolved absolute cw reflectance used for extraction of top-layer optics. One could do this by determining a calibration factor from measurements of optical phantoms with known optical properties. We determined the calibration factor by fitting the phantom measurements to the model results computed with the phantom coefficients. Three phantoms were used to define the calibration factor between the model results and the measured reflectance signal. The phantoms scanned the absorption and the scattering coefficients used in this study.

(2) Phase calibration was also needed to account for the phase errors caused by the instrument response. We calibrated the phase by performing phase measurements on a standard homogenous phantom with known optical coefficients and then calculating the expected theoretical phase (θ_{th}) for the calibration phantom's optical properties. The instrument phase error (θ_{in}) was then estimated from $\theta_{in} = \theta_{cal} - \theta_{th}$, where θ_{cal} is the phase obtained by the measurements of the calibration phantom. The calibration phantom's optical properties were $\mu_a = 0.005\ \text{mm}^{-1}$ and $\mu_s = 0.95\ \text{mm}^{-1}$. For stable and accurate results the apparatus was calibrated before each set of measurements was made.

4. Results and Discussion

In this section we present and discuss the results that we obtained from fitting the low-noise simulated Monte Carlo reflectance profiles. Then we present and discuss the results of the experimental measurements performed on a number of two-layered optical phantoms.

A. Fitting to Monte Carlo Simulated Measurements

We generated low-noise Monte Carlo simulated spatially resolved cw and FD reflectance profiles for two-layer models with semi-infinite bottom layers that had different interface depths of 2–10 mm and intervals of 1 mm and optical properties. In particular, for each interface depth value we generated 20 reflectance profiles with different optical properties that spanned the ranges ($0.005 < \mu_a < 2\ \text{mm}^{-1}$ and ($0.6 < \mu_s < 3.5\ \text{mm}^{-1}$) used in our study. A Henyey–Greenstein phase function with $g = 0.8$ was used to generate the Monte Carlo reflectance profiles. The noise added to the amplitudes of the Monte Carlo reflectance profiles (cw data) was 0.5–6% for source–detector distances of 1 to 30 mm. For the phase delay (FD data) the added noise was 0.005°–0.15° for source–detector range distances of 5–30 mm. We also added +15% errors for the *a priori* known interface values to account for the irregular geometry of the interface layers in real tissues and for errors in estimating such interface depths by use of different measurements techniques. These data provided ideal measurements and were used to test the validity of the proposed technique and the apparatus selected for various two-layer geometries.

Figure 7 shows the fits of the two-layer reflectance amplitude data with the proposed method for two interface depths, 3.5 and 6 mm. The results show that fitting only part ($r < D1$) of the reflectance profiles can be sufficient to describe the top-layer reflectance, even for a small layer thickness. It also shows the applicability of the two-layer diffusion approximation model in describing the bottom-layer reflectance (for distances of >5 mm).

Figure 8 shows the effect of interface depth on the measurement accuracy of the top and bottom layers' fixed optical properties. As shown in Fig. 8, for short interface depths (<4 mm) the accuracy of the top-layer absorption is less than that of thicker interface

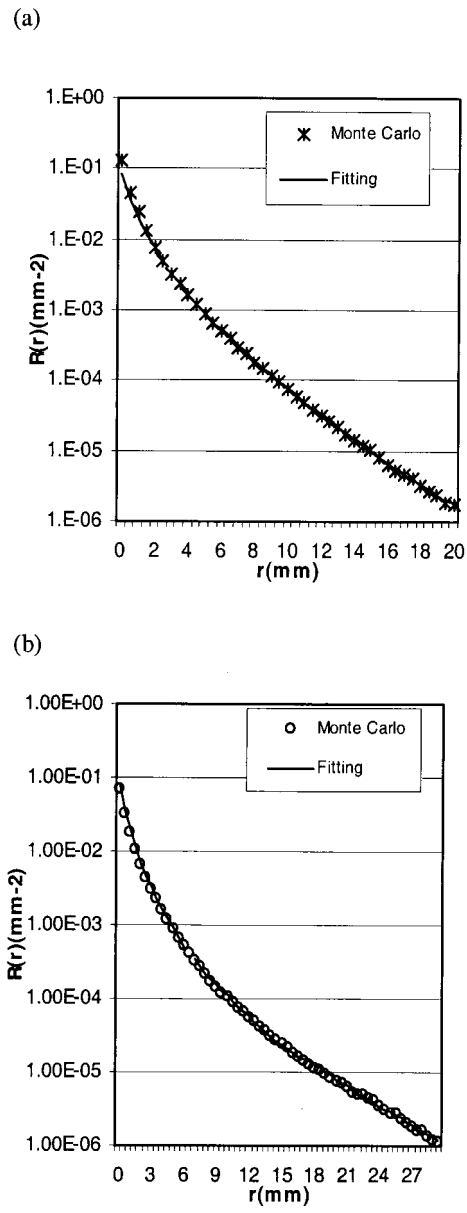

Fig. 7. Monte Carlo reflectance profiles versus results of fitting with the proposed method for (a) $l = 3.5$ mm, $\mu_{a2} = 0.005\ \text{mm}^{-1}$ (crosses) and (b) $l = 6$ mm, $\mu_{a2} = 0.02\ \text{mm}^{-1}$ (open circles). Other optical properties: $\mu_{a1} = 0.01$, $\mu_{s1} = 1.5$, $\mu_{s2} = 1.0$ [mm^{-1}].

depths (>5 mm). This is so mainly because of limitations on the position of the far detector needed in the spatially resolved reflectance measurements when one is investigating top-layer thicknesses of <4 mm. Our results agree with previous research results,[5,33,34,36] which show that obtaining the absorption coefficient from spatially resolved reflectance measured only at close source distances reduces the sensitivity and the accuracy of the results obtained. However, the accuracy in measurement of the other optical parameters including top-layer scattering shows insignificant changes with the interface depth of the top layer.

The mean and maximum errors in the estimated four optical parameters that characterize the two-

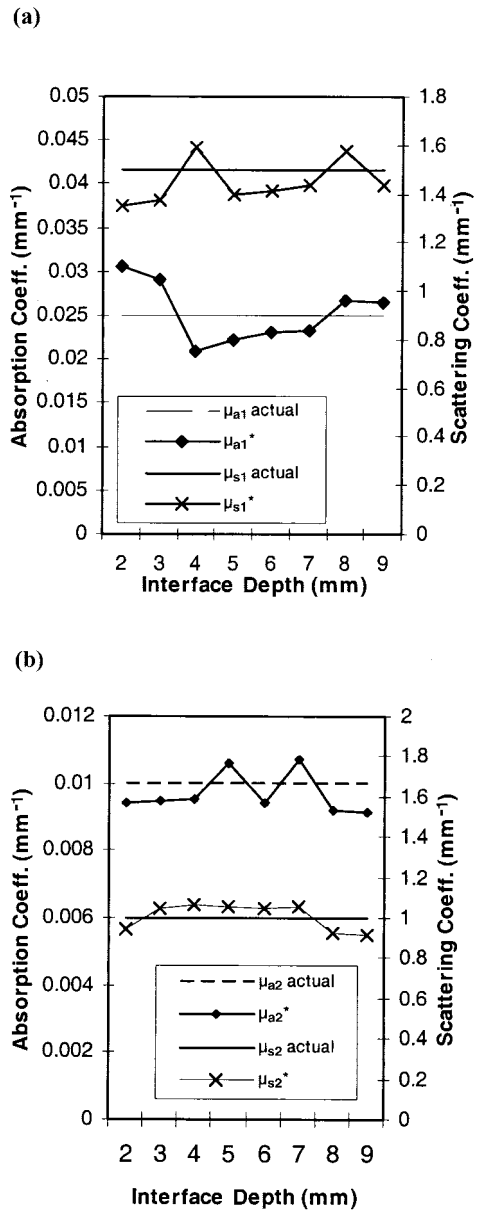

Fig. 8. Effects of varying the interface depth on the accuracy of (a) top-layer optical properties and (b) bottom-layer optical properties. Optical properties used to generate the simulated reflectance profiles are $\mu_{a1} = 0.025$, $\mu_{s1} = 1.5$, $\mu_{a2} = 0.01$, $\mu_{s2} = 1.0$ [mm^{-1}]; l = 2–10 mm.

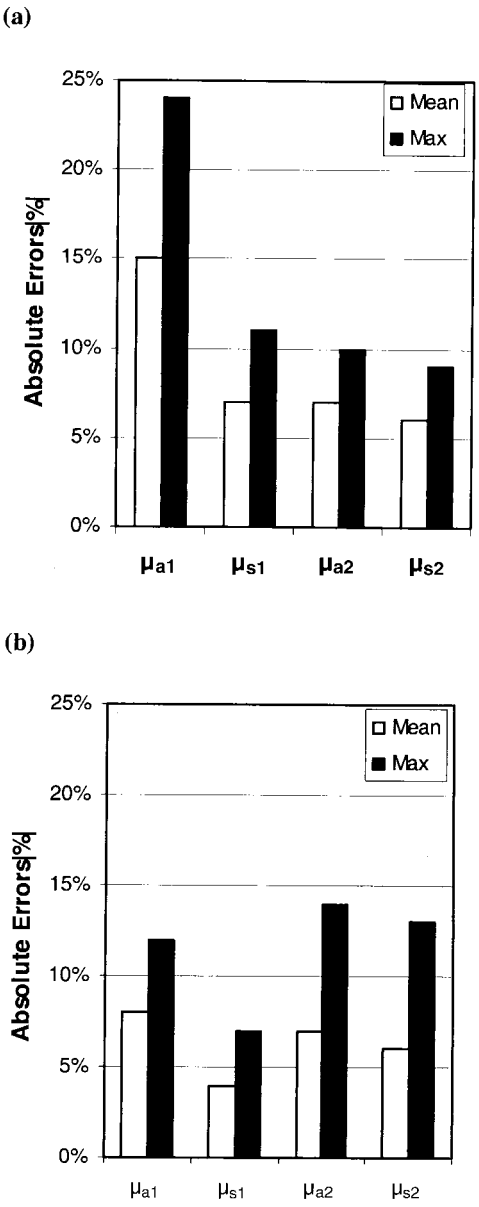

Fig. 9. (a) Absolute values for the mean and the maximum errors for interface depths 2 mm $< 1 <$ 5 m and (b) absolute values for the mean and the maximum errors for interface depths 5 mm $< l <$ 10 mm.

layer medium, namely, top-layer absorption and scattering coefficients μ_{a1} and μ_{s1} and bottom-layer absorption and scattering coefficients μ_{a2} and μ_{s2}, are summarized in Fig. 9. For top-layer thicknesses of $<$4 mm the mean error for the top-layer absorption is relatively high [~14%; Fig. 9(a)]. The maximum errors (~23%) result in very thin interface depths (~2 mm) and low absorption coefficients (0.005 mm^{-1}). Figure 9(b) shows the mean and maximum errors in the absolute optical properties for interface depths of 5–10 mm. The mean errors for estimating the top-layer properties were 8% and 4% for the absorption and scattering coefficients, respectively. The mean errors for estimating the bottom-layer properties were 7% and 6% for the absorption and scattering coefficients, respectively. In addition, if the only *a priori* information about the interface depth is that it is more than 5 mm, the actual interface depth can also be determined from the nonlinear regression results of the two-layer diffusion model, although with relatively higher errors of 15–20%. Thus, for such a range of interface depths (5–10 mm) the five optical properties that characterize this two-layer geometry can be estimated with reasonable inaccuracy ($<$20%) within a relatively short time (~1 min).

It should be noted that the concept of the Monte Carlo diffusion hybrid model[21] is included implicitly in such a method. Although the accuracy of measurement of the estimated top-layer absorption is less

than that obtained from the hybrid Monte Carlo diffusion model calculations,[22] the time needed to estimate all the optical parameters is greatly reduced.

However, an important conceptual problem in this method is that the accuracy of measurement of the bottom-layer optics can be influenced by the errors in estimating the top layer's optical properties. As was shown above, the top-layer errors can be as large as ~20% for two-layer models with thin top layers (2–3 mm). In addition, these top-layer estimation errors increased more in a clinical context because of the effect of the contact probe on absolute reflectance measurements and because of the deviation of the actual phase function from the assumed Henyey–Greenstein phase function. Thus it is of particular importance to evaluate the influence of such top-layer errors on the estimated bottom-layer optics. We did so by performing bottom-layer fittings for a number (~50) of two-layer models that had different optical properties and top-layer thicknesses within the range used in our study. The optical properties known *a priori* were used in the fitting after errors of 10–80% were added. We determined the errors in top-layer optics that result in bottom-layer errors of >20%, the standard for acceptable uncertainty for most of the qualitative assessments when ideal measurements are assumed. Initial fitting results showed that the influence of top-layer errors on bottom-layer errors depends to a large extent on the top layer's thickness. We found that, for top-layer thicknesses of 2–6 mm, errors of 50–60% in top-layer optics will result in errors in bottom-layer optics of >20%. For top-layer thicknesses greater than 7 mm the influence of top-layer errors on bottom-layer errors increases; it is maximum for top-layer thicknesses of ~10 mm. Errors of 35–50% in top-layer optics result in errors in bottom-layer optics of >20%.

We can conclude from these results that, assuming ideal measurements, the method should be useful for a two-layer model with a top-layer thickness of $l > 5$ mm. However, for a two-layer model with a thin top layer ($l < 5$ mm) the results obtained showed relatively high errors for the top layer absorption coefficients as a result of the use of reflectance measurements performed mainly at close source–detector distances only (i.e., near-source measurements). It should be noted that for two-layer media with $l < 5$ mm and with different phase functions other than the Henyey–Greenstein phase function that is used in the analysis, the errors in the top-layer absorption may increase even more, and additional *a priori* phase-function information, for example, $1 - g_1/1 - g_2$,[37,38] may be needed for fitting results with reasonable accuracy. In addition, when the aim is to measure the bottom-layer optics through an intervening top layer, the method can be useful for any two-layer model with 2–10-mm top-layer thickness.

Table 1. Three Two-Layer Phantoms Used for Experimental Measurements

	Phantom		
Optical Property	PH1	PH2	PH3
μ_{a1} (mm^{-1})	0.05	0.025	0.125
μ_{s1} (mm^{-1})	1.5	1.5	1.5
μ_{a2} (mm^{-1})	0.005	0.025	0.025
μ_{s2} (mm^{-1})	0.95	3.5	0.48
L (mm)	5	10	2

B. Fitting to Measurements on Two-Layer Phantoms

Experimental measurements of tissue-simulating optical phantoms were made to validate and test the proposed technique. For this purpose we used three two-layered solid phantoms with different interface depths (l = 2, 5, 10 mm) and different optical prop-

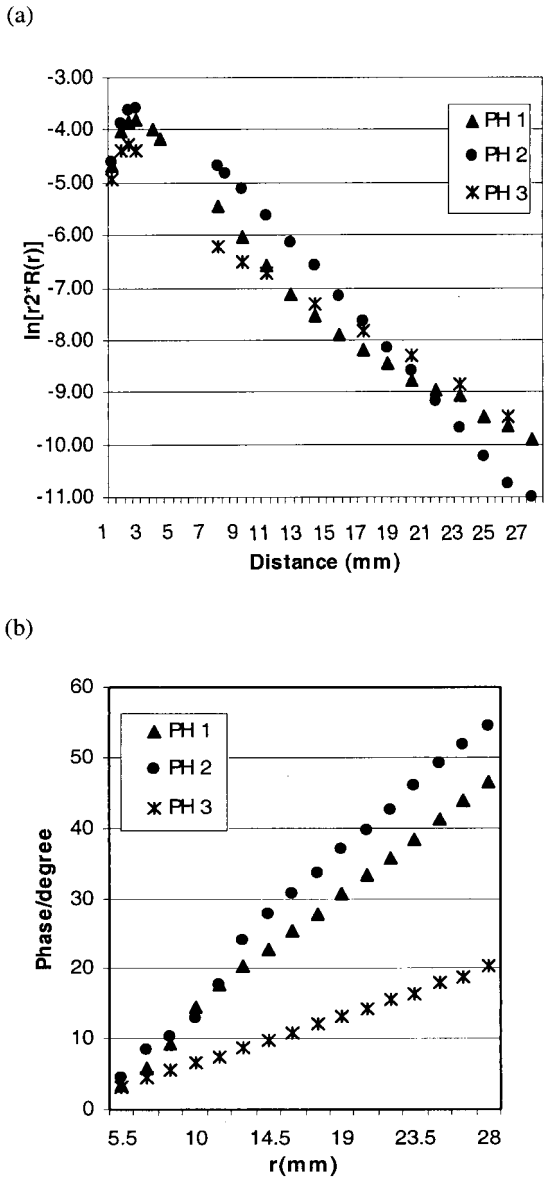

Fig. 10. Experimental data obtained from phantoms PH1, PH2, and PH3 reflectance measurements: (a) cw reflectance measurement, (b) phase-delay measurements.

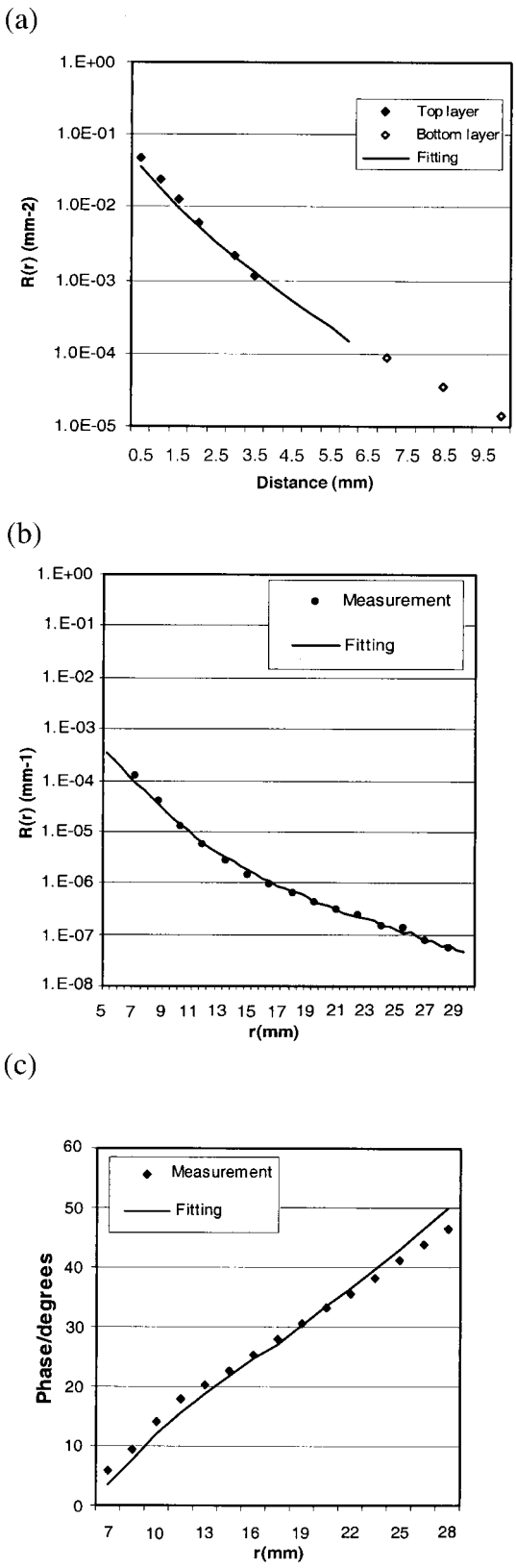

Fig. 11. PH1 fitting results: (a) top-layer cw reflectance fitting, (b) bottom-layer cw reflectance fitting, (c) bottom-layer phase-delay fitting.

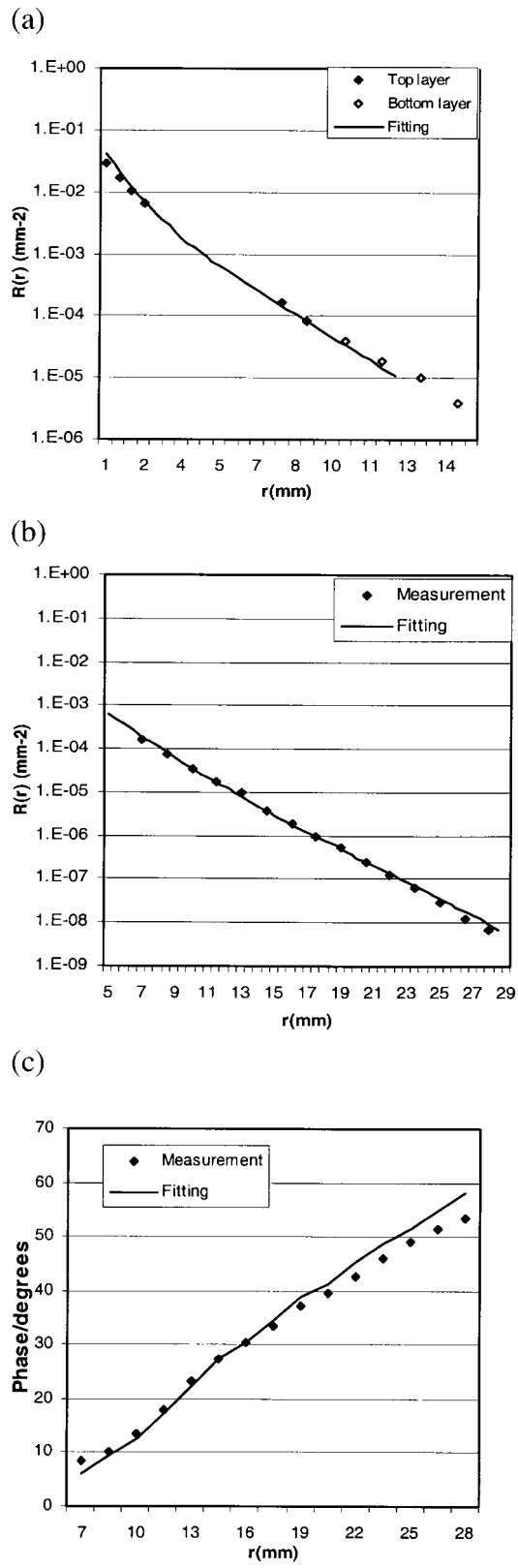

Fig. 12. PH2 fitting results: (a) top-layer cw reflectance fitting, (b) bottom-layer cw reflectance fitting, (c) bottom-layer phase-delay fitting.

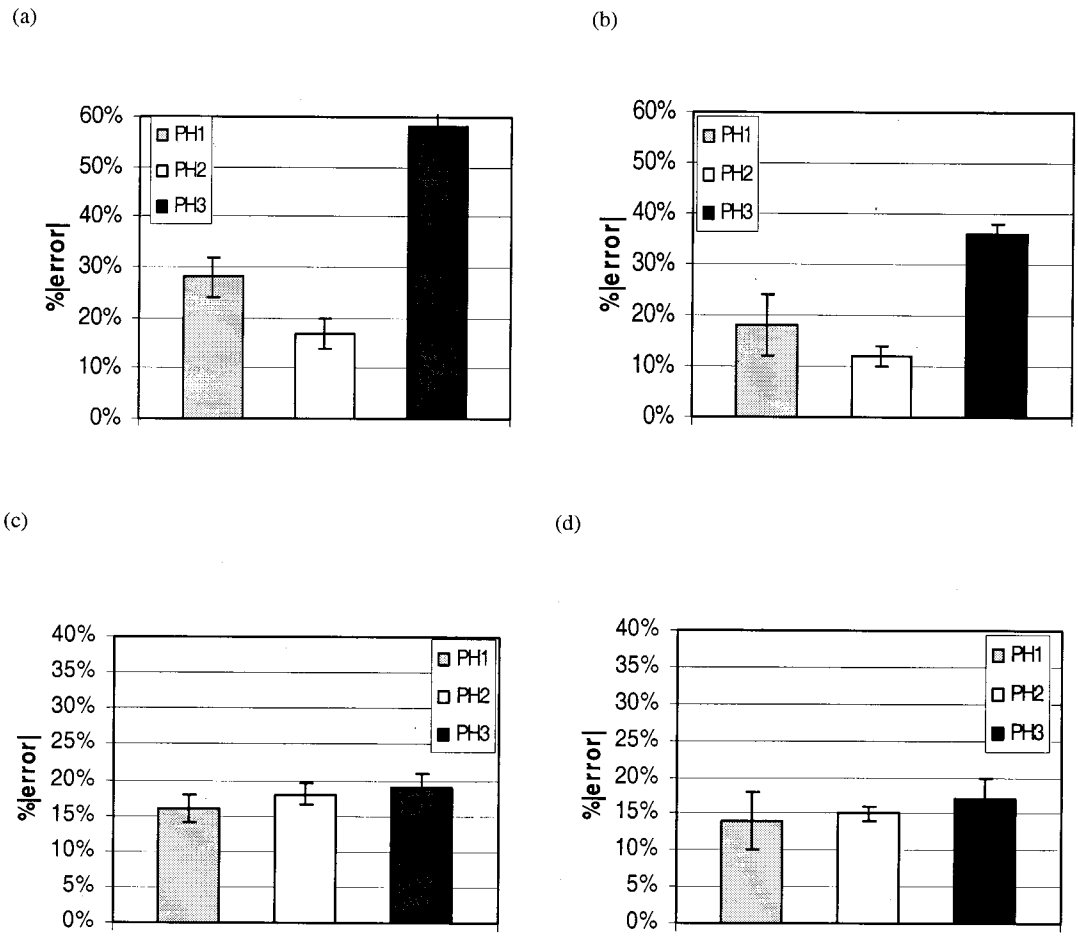

Fig. 13. Absolute errors in measurement of the phantoms' optical properties: (a) top-layer absorption, (b) top-layer scattering, (c) bottom-layer absorption, (d) bottom-layer scattering coefficients.

erties (at 630-nm wavelength), as summarized in Table 1.

The optical properties of the first phantom (PH1) and of the third phantom (PH3) approximately simulate those of dark skin and of the underlying layer of fat and muscle, respectively.[22,36] The optical properties and top-layer thicknesses of the second phantom (PH2) simulate to some extent those of the adult brain and the overlying skin and skull tissues (thickness, ~10 mm).[16,17]

The results of the measurements (phase and reflectance) performed on the three phantoms (PH1, PH2, and PH3) are shown in Fig. 10. The errors in the reflectance measurements are in the range 3–5% along radial distances of 5–28 mm. The use of a high-gain silicon photodiode with an ~82-dB linear response with the digital phase-detection method results in typical phase-measurement errors of 0.5° along radial distances of 5–20 mm and increase to 0.8° for radial distances greater than 20 mm. The effect of the highly absorbing top layer in PH3 appeared in the reflectance amplitude attenuation; those of PH1 and PH2 appeared for near-source distances. However, the reflectance profile for PH3 increased (for $r > 10$ mm) because of the low attenuation coefficient of the phantom bottom layer. We can observe from Fig. 10 the slope of the measured reflectance profile for PH2 that is steeper than those of PH1 and PH3 as a result of the highly scattering bottom layer of this phantom. We fitted the three phantoms' experimental measurements (reflectance and phase), using the proposed method. The maximum time needed for the apparatus to measure and estimate each of the optical properties of the phantoms is less than 1 min. The fits of the experimental measurements (reflectance and phase) obtained from phantoms 1 and 2 are shown in Figs. 11 and 12, respectively. As shown in Figs. 11 and 12, we have used mostly far-distance (>5 mm) measurements in fitting the bottom-layer optics of phantoms with thick top layers. We did this to increase the bottom layer's fractional signal contribution to the total detected signal, thus increasing the accuracy of the bottom-layer optics required. In addition, theoretical results have shown that the inclusion of near source distance when one is fitting the two-layer diffusion model does not improve or significantly affect the accuracy of the bottom-layer optics obtained.

The errors in the estimated optical parameters obtained from the fitting results are summarized in Fig. 13. The accuracy of the optical parameters of PH1 was ~15% for the bottom layers. For the top layer

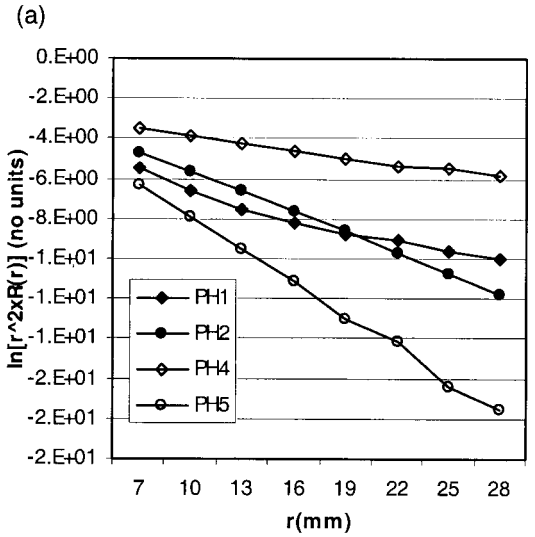

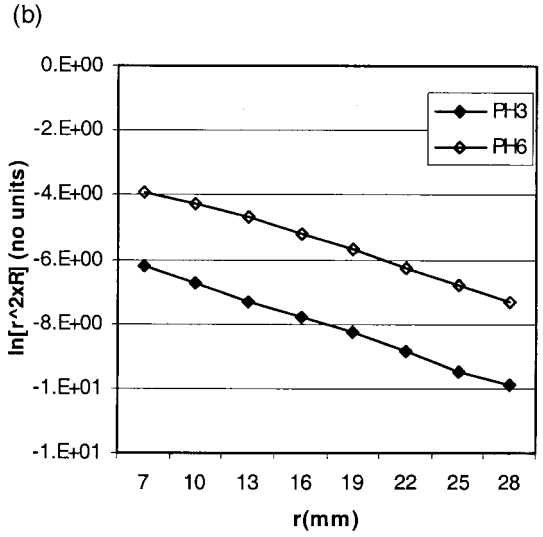

Fig. 14. Reflectance measured at far distances (>8 mm) for the six phantoms.

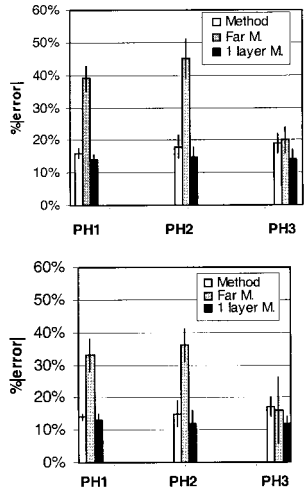

Fig. 15. Absolute errors of the bottom-layer optical properties (absorption, top; scattering, bottom) of PH1, PH2, and PH3 as obtained from three measurement techniques.

the errors increased to ~18% and ~28% for the scattering and absorption coefficients, respectively. For PH2 the fitting of the bottom optical properties resulted in errors of ~15% and ~18% for the scattering and the absorption coefficients, respectively. For the top layer the errors were ~12% and ~17% for the scattering and the absorption coefficients, respectively. Fitting of PH3 reflectance and the phase measurements with the proposed method (results not shown) has not produced satisfactory results (~50% errors) for the top-layer optical properties. However, the inaccuracy of the bottom-layer optical properties is (<20%) in spite of the large errors measuring in the top layer's properties, as shown in Fig. 13. We also present measurements of semi-infinite phantoms PH4, PH5, and PH6, which have the same bottom-layer optical properties as PH1, PH2, and PH3, respectively. Such measurements of semi-infinite phantoms serve as hypothetical measurements made directly of the bottom-layer optics of the two-layer phantoms used in our study. As shown in Fig. 14, the effect of the overlying top layer on the reflectance profile is significant for the slope of the ln r^2R reflectance measured for PH1 and PH2. The effect is maximum for PH2 and minimum for PH3. We also compared the accuracy of the phantoms' bottom-layer optics obtained with the proposed measurement method with those obtained from measurement at only far-source–detector distances (>1.5 cm) and for use of the semi-infinite diffusion model for fitting.

The error results that we obtained from measurements with semi-infinite phantoms PH4, PH5, and PH6 are summarized in Fig. 15 for comparison. The results in Fig. 15 show that obtaining the bottom layer from far-detector measurements does not provide a real estimate (errors of as much as ~50%) of the optical properties of that layer, and the effect of the top layer should also be taken into consideration during analysis of PH1 and PH2 reflectance measurements. The results also show that the proposed method accounts for the top-layer effect and estimates the bottom layer's optical properties with accuracies comparable with those obtained with hypothetical measurements made directly of the bottom layer with the top layer removed (the semi-infinite phantoms).

5. Conclusions

We have presented a method based on statistics on the propagation of photons within certain depths inside tissues for obtaining the optical properties of two-layer turbid media. We have developed a reflectance apparatus that extracts the top layer's reflectance separately from the spatially resolved absolute cw reflectance and then extracts the bottom layer's optical properties from the relative frequency-domain reflectance. Although the method can be used with two-layer geometry that has a top-layer thickness of

$l < 4$ mm, providing *a priori* phase-function information, its optimum applicability in practice appears to be for tissues with top-layer thicknesses of >5 mm. Such a model can simulate many-layered tissues such as muscle and overlying tissues or brain and overlying skull tissues. The method has also proved to be useful when the aim was to measure only the bottom layers of tissues with superficial layer thickness l (2–10 mm), for example, in measuring muscle oxygenation through thick overlying layers of skin and fat. For such geometries the effect of top-layer on bottom-layer reflectance is significant because the bottom layer's optical properties cannot be determined accurately from measurements of the far-source–detector distance, and the effect of overlying layers should be quantified. The method can be extended and used to investigate multilayer tissues with n number of layers with known thickness. With this approach the time needed to extract the optical properties of a multilayer turbid medium can be greatly reduced. That this is so can be explained conceptually because we transform the domain of search in the inverse problem from searching for $2n$ parameters simultaneously to searching for only two parameters simultaneously n number of times. The reduction of time is more significant in increasing the number of layers that characterize the multilayer media. The apparatus and method described here can easily be used with any multilayer tissues (more than two layers) by selection of a limiting source–detector position for each layer and generation of frequency-resolved (100–1000-MHz) reflectance profiles such that the nth-layer optical properties could be estimated from these frequency-resolved reflectance profiles measured at the corresponding detector position (dn), assuming the $n - 1$ layer properties previously deduced sequentially. Future research will involve applying the method to three- and four-layer phantoms with particular focus on the geometry of the brain and overlying tissues.

The authors thank Amr Hendi, Amr Bagdadi, and Yasser Abd Aziz for technical assessment. The authors also thank Ronald Bays and Alwin Kienle for the scientific discussion about the phantoms' properties and the theory of light transport in tissues. This work was funded and supported by the R&D department at International Electronics Co. and by the National Institute of Laser at Cairo University.

References

1. R. A. J. Groenhuis, H. A. Ferwerda, and J. J. Ten Bosch, "Scattering and absorption of turbid materials determined from reflection measurements," Appl. Opt. **22,** 2456–2467 (1983).
2. B. C. Wilson, T. J. Farrell, and M. S. Patterson, "An optical fiber-based diffuse reflectance spectrometer for non-invasive investigation of photodynamic sensitizers *in vivo*," in *Future Directions and Application in Photodynamic Therapy*, G. J. Gomer, ed., Vol. IS06 of SPIE Institute Series (SPIE, Bellingham, Wash., 1990), pp. 219–231.
3. M. G. Nichols, E. L. Hull, and T. H. Foster, "Design and testing of a white-light steady-state diffuse reflectance spectrometer for determination of optical properties of highly scattering systems," Appl. Opt. **36,** 1–12 (1997).
4. A. Kienle, L. Lilge, M. S. Patterson, R. Hibst, R. Steiner, and B. C. Wilson, "Spatially resolved absolute diffuse reflectance measurements for noninvasive determination of the optical scattering and absorption coefficients of biological tissue," Appl. Opt. **35,** 2304–2314 (1996).
5. J. S. Dam, C. B. Pedersen, T. Dalgaard, P. E. Fabricius, P. Aruna, and S. A. Engels, "Fiber-optic probe for noninvasive real-time determination of tissue optical properties at multiple wavelengths," Appl. Opt. **40,** 1155–1164 (2001).
6. B. W. Pogue and M. S. Patterson, "Frequency-domain optical absorption spectroscopy of finite tissue volumes using diffusion theory," Phys. Med. Biol. **39,** 1157–1180 (1994).
7. A. Kienle and M. S. Patterson, "Determination of the optical properties of semi-infinite turbid media from frequency-domain reflectance close to the source," Phys. Med. Biol. **42,** 1801–1819 (1997).
8. M. Gerken and G. W. Faris, "High-accuracy optical property measurements using a frequency domain technique," in *Optical Tomography and Spectroscopy of Tissues III*, B. Chance, R. R. Alfano, and B. Tromberg, eds., Proc. SPIE **3597,** 593–600 (1999).
9. S. L. Jacques, "Time-resolved reflectance spectroscopy in turbid tissues," IEEE Trans. Biomed. Eng. **36,** 1155–1161 (1989).
10. S. J. Madsen, B. C. Wilson, M. S. Patterson, Y. D. Park, S. C. Jacques, and Y. Hefetz, "Experimental tests of a simple diffusion model for the estimation of scattering and absorption coefficients of turbid media from time-resolved diffuse reflectance measurements," Appl. Opt. **31,** 3509–3517 (1992).
11. T. J. Farrell, M. S. Patterson, and M. Essenpries, "Influence of layered tissue architecture on estimates of tissue optical properties obtained from spatially resolved diffuse reflectometry," Appl. Opt. **37,** 1958–1972 (1998).
12. G. Alexandrakis, T. J. Farrell, and M. S. Patterson, "Accuracy of the diffusion approximation in determining the optical properties of a two-layer turbid medium," Appl. Opt. **37,** 7401–7410 (1998).
13. A. Kienle, L. Lilge, M. S. Patterson, B. C. Wilson, R. Hibst, and R. Steiner, "Investigation of multi-layered tissue with *in-vivo* reflectance measurements," in *Photon Transport in Highly Scattering Tissue*, S. Avrillier, B. Chance, G. J. Mueller, A. V. Priezzhev, and V. V. Tuchin, eds., Proc. SPIE **2326,** 212–221 (1995).
14. A. Kienle, M. S. Patterson, N. Dognitz, R. Bays, G. Wagnieres, and H. Bergh, "Noninvasive determination of the optical properties of two-layered turbid media," Appl. Opt. **37,** 779–791 (1998).
15. M. A. Franceschini, S. Fantini, L. A. Paunescu, J. S. Maier, and E. Gratton, "Influence of superficial layer in the quantitative spectroscopic study of strongly scattering media," Appl. Opt. **37,** 7447–7458 (1998).
16. E. Okada, M. Firbank, and D. T. Delpy, "The effect of overlying tissue on the spatial sensitivity profile of near-infrared spectroscopy," Phys. Med. Biol. **40,** 2093–2108 (1995).
17. M. Hibroka, M. Firbank, M. Essenpries, M. Cope, S. R. Arridge, P. Zee, and D. T. Delpy, "A Monte Carlo investigation of optical pathlength in inhomogeneous tissue and its application to near-infrared spectroscopy," Phys. Med. Biol. **38,** 1859–1876 (1993).
18. R. J. Hunter, M. S. Patterson, T. J. Farrell, and J. E. Hayward, "Haemoglobin oxygenation of a two-layer tissue-simulating phantom for time-resolved reflectance: effect of top layer thickness," Phys. Med. Biol. **47,** 193–208 (2002).
19. T. H. Pham, T. Spott, L. O. Svaasand, and B. J. Tomberg, "Quantifying the properties of two-layer turbid media with frequency-domain diffuse reflectance," Appl. Opt. **39,** 4733–4745 (2000).

20. G. Alexandrakis, R. A. Weersink, J. T. Bruulsema, and M. S. Patterson, "Estimation of the optical properties of two-layer tissue simulating phantoms from spatially resolved frequency-domain reflectance," in *Optical Tomography and Spectroscopy of Tissues III*, B. Chance, R. R. Alfano, and B. Tromberg, eds., Proc. SPIE **3597,** 155–163 (1999).
21. G. Alexandrakis, T. J. Farrell, and M. S. Patterson, "Monte Carlo diffusion hybrid model for photon migration in a two-layer turbid medium in the frequency domain," Appl. Opt. **39,** 2235–2244 (2000).
22. G. Alexandrakis, D. R. Busch, G. W. Faris, and M. S. Patterson, "Determination of the optical properties of two-layer turbid media by use of a frequency-domain hybrid Monte Carlo diffusion model," Appl. Opt. **40,** 3810–3821 (2001).
23. G. H. Weiss, R. Nossal, and R. F. Bonner, "Statistics of penetration depth of photons reemitted from irradiated tissue," J. Mod. Opt. **36,** 349–359 (1989).
24. M. S. Patterson, S. Anderson, B. C. Wilson, and E. K. Osei, "Absorption spectroscopy in tissue-simulating materials: a theoretical and experimental study of photon paths," Appl. Opt. **34,** 22–30 (1995).
25. J. C. Schotland, J. C. Haselgrove, and J. S. Leigh, "Photon hitting density," Appl. Opt. **32,** 448–453 (1993).
26. H. Martens and T. Naes, *Multivariate Calibration* (Wiley, New York, 1994).
27. B. C. Wilson and G. Adam, "A Monte Carlo model for the absorption and flux distributions of light in tissue," Med. Phys. **10,** 824–830 (1983).
28. S. A. Prahl, M. Keijzer, S. L. Jacques, and A. J. Welch, "A Monte Carlo model of light propagation in tissue," in *Dosimetry of Laser Radiation in Medicine and Biology*, G. Mueller and D. Sliney, eds., Vol. IS5 of SPIE Institute Series (SPIE, Bellingham, Wash., 1989), pp. 102–111.
29. W. H. Press, S. A. Teukolsky, W. T. Vetterling, and B. P. Flannery, *Numerical Recipes in C—The Art of Scientific Computing*, 2nd ed. (Cambridge U. Press, London, 1992).
30. R. C. Haskel, L. O. Svaasand, T. T. Tasy, T. C. Feng, M. McAdams, and B. J. Tromberg, "Boundary conditions for the diffusion equation in radiative transfer," J. Opt. Soc. Am. A **11,** 2727–2741 (1994).
31. B. Chance, M. Cope, E. Gratton, N. Ramanujam, and B. Tromberg, "Phase measurements of light absorption and scatter in human tissue," Rev. Sci. Instrum. **69,** 3457–3481 (1998).
32. C. S. Burrus, J. H. McClellan, A. V. Oppenheim, T. W. Parks, R. W. Schafer, and H. W. Schuessler, *Computer-Based Exercises for Signal Processing Using Matlab* (Prentice-Hall, Englewood Cliffs, N.J., 1994).
33. J. R. Mourant, I. J. Bigio, D. A. Jack, and T. M. Johnson, "Measuring absorption coefficients in small volumes of highly scattering media: source–detector separations for which path lengths do not depend on scattering properties," Appl. Opt. **36,** 5655–5661 (1997).
34. G. Kumar and J. M. Schmitt, "Optimal probe geometry for near-infrared spectroscopy of biological tissue," Appl. Opt. **36,** 2286–2293 (1997).
35. R. Bays, G. Weorgers, D. Robert, J. Theumann, A. Vitkin, J. Savary, P. Monnier, and H. van den Bergh, "Three-dimensional optical phantom and its application in photodynamic therapy," Lasers Surg. Med. **21,** 227–234 (1997).
36. S. Yeh and O. S. Khalil, "Multivariate method for the determination of tissue optical properties from diffuse reflectance profiles," in *Optical Tomography and Spectroscopy of Tissues III*, B. Chance, R. R. Alfano, and B. Tromberg, eds., Proc. SPIE **3597,** 456–464 (1999).
37. F. Bevilacqua, D. Piguet, P. Marquet, and B. J. Tromberg, "*In-vivo* local determination of tissue optical properties," in *Photon Propagation in Tissues III*, D. Benaron, B. Chance, and M. Ferrari, eds., Proc. SPIE **3194,** 262–268 (1997).
38. F. Bevilacqua and C. Depeursinge, "Monte Carlo study of diffuse reflectance at source–detector separations close to one transport mean free path," J. Opt. Soc. Am. A **16,** 2935–2945 (1999).